Vortex-controlled morphology conversion of microstructures on silicon induced by femtosecond vector vortex beams

Huachao Cheng, Peng Li, Sheng Liu, Peng Chen, Lei Han, Yi Zhang, Wei Hu, and Jianlin Zhao

Citation: Appl. Phys. Lett. **111**, 141901 (2017); doi: 10.1063/1.4994926
View online: http://dx.doi.org/10.1063/1.4994926
View Table of Contents: http://aip.scitation.org/toc/apl/111/14
Published by the American Institute of Physics

APPLIED PHYSICS LETTERS **111**, 141901 (2017)

Vortex-controlled morphology conversion of microstructures on silicon induced by femtosecond vector vortex beams

Huachao Cheng,[1,a)] Peng Li,[1,a)] Sheng Liu,[1,b)] Peng Chen,[2] Lei Han,[1] Yi Zhang,[1] Wei Hu,[2] and Jianlin Zhao[1,b)]

[1]*MOE Key Laboratory of Material Physics and Chemistry under Extraordinary Conditions, and Shaanxi Key Laboratory of Optical Information Technology, School of Science, Northwestern Polytechnical University, Xi'an 710072, China*

[2]*National Laboratory of Solid State Microstructures and College of Engineering and Applied Sciences, Nanjing University, Nanjing 210093, China*

(Received 8 July 2017; accepted 19 September 2017; published online 2 October 2017)

We demonstrate the morphology conversion of surface microstructures on silicon induced by femtosecond vector vortex beams. By tuning the topological charge of the vortex phase carried by the vector beam, we achieve the transition of ablation crater between subwavelength ripples and hole, and the switching of ripple orientation. It is shown that the vortex phases give rise to the converting of the two polarization components of the focused vector beams, and produce dramatically different polarization and intensity distributions in the focal fields. Such vortex-dependent focal fields of femtosecond vector beams are experimentally generated to realize the morphology conversion of surface microstructures on silicon. Our results not only enable the realization of manipulating the laser-induced morphology but also support the visualized mapping of the polarization state of the focused vector beams. *Published by AIP Publishing.*
https://doi.org/10.1063/1.4994926

Femtosecond laser induced periodic surface structure (LIPSS, often termed "ripples") has drawn extensive attentions during past decades, because of the convenience in fabricating micro- and nano-scale structures. In particular, these structures can be formed in many materials after several laser pulses irradiating.[1–3] On this basis, a variety of impressive components have been fabricated, such as nano-gratings,[4] bionic surface structures,[5,6] and birefractive plates.[7–9] Meanwhile, the formation mechanism and the dependence of LIPSS on the incident laser beams have been intensively studied.[10–13] There is a common view that the orientation of the ripples is locked to the polarization state of the incident beam. Namely, when the linearly polarized laser pulses have energy slightly above the ablation threshold of the target, the ripples with orientation perpendicular to the polarization direction of irradiation beams will be formed.[1–4]

Owing to this polarization-locking property, femtosecond laser beams with spatially inhomogeneous states of polarization, i.e., femtosecond vector beams, have been proposed to fabricate and manipulate complex morphologies.[14–19] Importantly, the tightly focused vector beams can yield the sub-diffraction sized spots and the enhanced longitudinal components,[20] which exhibit intriguing prospect in laser-matter interactions.[14] On the other hand, the intensity profile of the incident laser beam also plays a crucial role in determining the laser-induced morphology. One of the most typical examples is the femtosecond vortex beam with doughnut profile. It has been demonstrated to create subwavelength ring-shaped craters on silicon or glass,[21] and construct complex morphologies on metals, twisted nanoneedles,[22,23] and spiral structures.[24] Predictably, utilizing spatially structured beams to directly fabricate surface microstructures is emerging as a fascinating possibility and a potential approach in manufacturing functional components with complex surface structures.

In this letter, we simultaneously introduce the spatially topological structures of polarizations and phases into femtosecond laser beams, to directly fabricate and flexibly manipulate the surface structure morphology upon silicon wafer. Utilizing a phase-type spatial light modulator (SLM) and a q-plate, we generate femtosecond vector vortex beams and focus them on silicon surface to induce damage morphology. By varying the topological charge of vortex phase, the vortex-dependent morphology conversion is experimentally observed. To reveal the underlying physical mechanism, we numerically analyze the focal field properties of vector vortex beams by means of vectorial diffraction integration.

Figure 1 schematically shows the detailed experimental setup. A Ti:sapphire regenerative amplifier system (Spectral Physics, Spitfire ACE-35F) is used as the laser source to generate linearly polarized femtosecond laser pulses, with pulse duration about 35 fs, central wavelength at 800 nm, and reputation rate of 1 kHz. After passing through the elements shown in the dashed line rectangle of Fig. 1, the output laser is first corrected into a high-purity linearly polarized Gaussian beam, with its power continuously adjusted via the half-wave plate (HWP1). The collimated beam is transformed into a radially or azimuthally polarized vortex beam under the sequential modulation of a reflected phase-type SLM (Hamamatsu, x11840-02) and a q-plate ($q = 1/2$). Finally, it is focused on the surface of silicon wafer via a $10\times$ microscope object (NA = 0.25). The pulse number is adjusted by an electronic shutter before the object.

[a)]H. Cheng and P. Li contributed equally to this work.
[b)]Electronic addresses: shengliu@nwpu.edu.cn and jlzhao@nwpu.edu.cn

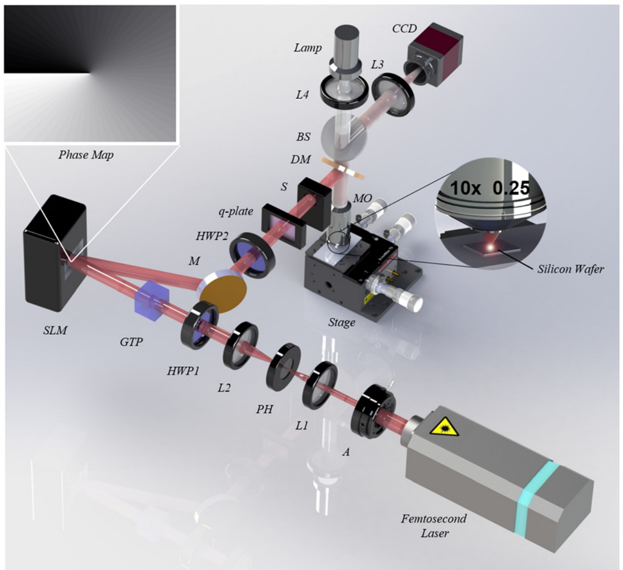

FIG. 1. Schematic of the experimental setup. A, aperture; L1-L4, lenses; PH, pinhole; HWP, half-wave plate; GTP, Glan-Tylor prism; SLM, spatial light modulator; M, mirror; *q*-plate, phase retardation element; S, shutter; DM, dichroic mirror; MO, microscope object; BS, beam splitter; and Lamp, white light source. Insets: phase map located on SLM (top left corner) and zoom-in view of radiation region (right).

In practice, a phase map (the inset of Fig. 1, gray-scale from 0 to 255 corresponding to phase value from 0 to 2π) is loaded on the SLM, and the refractive index of which is modulated as the loaded image; thus, the phase information of the phase map is imparted into the input beams, converting the Gaussian beam into a vortex beam, of which the topological charge can be changed by loading different phase maps. The *q*-plate is a type of liquid crystal element with azimuthally variant phase retardation, manufactured with photoalignment technique.[25–27] Combining with the half-wave plate (HWP2), the *q*-plate can transform the linearly polarized vortex beam into a radially or azimuthally polarized vortex beam. The silicon wafer is mounted on a 3-axis stage (Thorlabs, MAX302), and the irradiated region is real-time monitored by a confocal microscopy system.

Experimentally, we irradiate the silicon using a radially polarized beam without vortex phase (the topological charge $l=0$), and modulate the laser fluence to a value slightly above the ablation threshold (about 0.35 J/cm^2 before the microscope object). After that, the vortex phase with $l \neq 0$ is attached to the vector beam by loading the corresponding phase map (the phase range is 0–$2\,l\pi$). After being exposed by the focused vector vortex beam with 100 pulses in air environment, the silicon wafer was examined by a scanning electron microscope (SEM). Figure 2 shows the SEM images of surface structures on the sample, where the upper and lower rows correspond to the radially and azimuthally polarized vortex beams with $l=0$, 1, and 10, respectively. We can clearly find that, when irradiated by the vector beams without vortex phase ($l=0$), surface ripples with period around 0.6 μm can be observed at the irradiated regions, and the ripple orientate perpendicular to the local polarization direction of incident beams. Namely, the radially and azimuthally polarized beams induce ring-shaped and radial-shaped ripples, respectively, as shown in Figs. 2(a_1) and 2(b_1). When $l=1$, as shown in Figs. 2(a_2) and 2(b_2), the irradiated regions exhibit single hole-shaped craters, and the sizes of hole-shaped craters are almost same as that of the central areas without ripples for the cases of $l=0$. When the topological charge further increased to $l=10$, the local orientations of induced ripples are parallel to the corresponding polarization directions of incident beams, which are perpendicular to the ripples corresponding to $l=0$, as shown in Figs. 2(a_3) and 2(b_3). Namely, the radially and azimuthally polarized vortex beams induce radial- and ring-shaped ripples, respectively. In addition, it should be noted that, as topological charge increases, the radius of annular irradiated regions correspondingly increases, giving rise to larger annular ablation crater, while the ripples almost keep the same periods (about 0.6 μm). This feature also verifies the common view that the period of ripple closely depends on the wavelength of incident beam.

The polarization-locking ripples can be explained in terms of interference between the incident beam and a surface plasmon polaritons (SPPs).[12] Femtosecond laser pulses

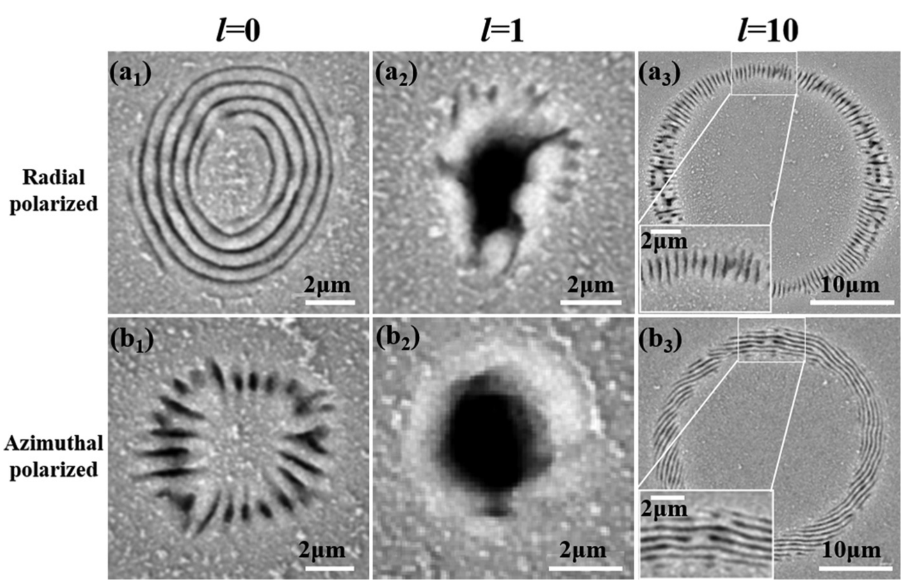

FIG. 2. SEM images of surface structures on silicon wafer induced by radially (upper) and azimuthally (lower) polarized vortex beams with topological charges of $l=0$, 1, and 10, respectively.

irradiated the sample surface, producing defects which satisfy the generation condition of SPPs, that is, the wave vector matching condition can be satisfied around the defects. Moreover, the high excited surfaces exhibit metallic properties after irradiation of intense femtosecond laser pulses. As a result, the SPPs can be generated and the electrons in surface oscillate along the polarization direction of incident field, causing periodic instability of the surface and finally forming ripples. When the incident beam is locally linearly polarized (radially and azimuthally polarized in our experiments), the oscillation of electrons is definite in the direction of polarization, and thus the ripples will be formed with orientation perpendicular to the polarization state. When the incident beam is circularly polarized, the polarization state is variant; as a result, the oscillation of electrons cannot be definite, and no ripples will be formed in irradiated area. Therefore, the laser-induced morphology conversion of surface microstructures shown in Fig. 2 is considered to be attributed to the polarization conversion induced by the vortex phase.

To reveal the intriguing morphology conversion of surface structures induced by the femtosecond vector vortex beams, we numerically analyze the focusing property of these beams based on Richards-Wolf theory.[28] Supposing the incident vector beam is focused by a lens, the electric field in the focal plane can be described as[29–31]

$$\begin{aligned}\mathbf{E}(r,\phi,z) &= \begin{pmatrix}\mathbf{E}_r\\ \mathbf{E}_\phi\\ \mathbf{E}_z\end{pmatrix} = -\frac{ikf}{2\pi}\int_0^{\theta_{\max}}\sin\theta d\theta\int_0^{2\pi}AP(\theta)\\ &\times\left[\cos\varphi_0\begin{pmatrix}\cos\theta\cos(\varphi-\phi)\mathbf{e}_r\\ 0\mathbf{e}_\phi\\ \sin\theta\mathbf{e}_z\end{pmatrix}\right.\\ &\left.+\sin\varphi_0\begin{pmatrix}0\mathbf{e}_r\\ \cos(\varphi-\phi)\mathbf{e}_\phi\\ 0\mathbf{e}_z\end{pmatrix}\right]\\ &\times\exp\{ik[z\cos\theta+r\sin\theta\cos(\varphi-\phi)]\}d\varphi,\end{aligned} \tag{1}$$

where (r, φ, z) denote the cylindrical coordinates in focal plane, θ and φ are the polar and azimuthal angles of focusing system, $\theta_{\max} = \arcsin(\mathrm{NA})$ is the maximum aperture of the focusing lens determined by the numerical aperture NA, A is the complex amplitude of the incident beam that includes the phase term $e^{il\varphi}$, and φ_0 is a constant phase defining the polarization state of incident beam ($\varphi_0 = 0$ and $\pi/2$ correspond to the radial and azimuthal polarizations, respectively); $P(\theta) = (\cos\theta)^{1/2}$ is the apodization function of the lens, $k = 2\pi/\lambda$ is the wave number, λ is the wavelength, and f is the focal length. It should be noted that, under the focusing condition in our experiment, NA = 0.25, so the longitudinally polarized components ($\mathbf{e}_z$) of the focal field, of which the energy accounts for about 3% of the total energy, can be neglected compared with the transversely polarized one ($\mathbf{e}_r$ and $\mathbf{e}_\phi$). Thus, we will only consider the transverse components $\mathbf{e}_r$ and $\mathbf{e}_\phi$ below.

Figure 3 displays the numerical calculation results of intensity, polarization, and phase distributions in focal plane of radially polarized vortex beams, where the first row shows the total intensity and polarization distributions of focal fields, the middle and bottom rows show the intensity and phase distributions of radial and azimuthal components, respectively. The calculated polarizations of the focal fields are marked by ellipses shown in the top row, where the red and green ellipses depict the right- and left-hand elliptical polarizations, respectively. In agreement with earlier studies,[30] the focal field of a radially polarized beam has a null azimuthal component, as shown in Fig. 3(a_1). Namely, the focal field is radially polarized. Correspondingly, the damage area, as shown in Fig. 2(a_1), is ring-shaped mapping the "bright" area in Fig. 3(a_1), of which the ripples orientate perpendicular to the local polarization expressed by the dashed line in Fig. 3(a_1). When $l = 1$, the azimuthal component dramatically increases; meanwhile, the radial component with a same peak power is formed, both of which carry the +1 charged spiral phase. Moreover, it is notable that the phase difference of the radial and azimuthal components is $\pi/2$ at the region of central spot, and $-\pi/2$ at the region of ring spot. This gives rise to the polarization distribution as shown in Fig. 3(b_1), which has a circularly polarized singularity in the center, and the polarization ellipticity varies along the radial direction. It can be noted that, in the central area where the energy exceeds the ablation threshold, the focal field is circularly polarized, as previously reported, circular polarized beam cannot form ripples,[13] so the fabricated microstructure is an ablated hole without any ripples, as shown in Fig. 2(a_2). Particularly interesting is the case of $l = 10$, as also shown in the results of Fig. 3(c), the main energy is transited from the radial component to the azimuthal one, and the focal field is almost converted to the azimuthally polarized one. Correspondingly, the ablated microstructure with radial-shaped ripples [see Fig. 2(a_3)] is produced, which

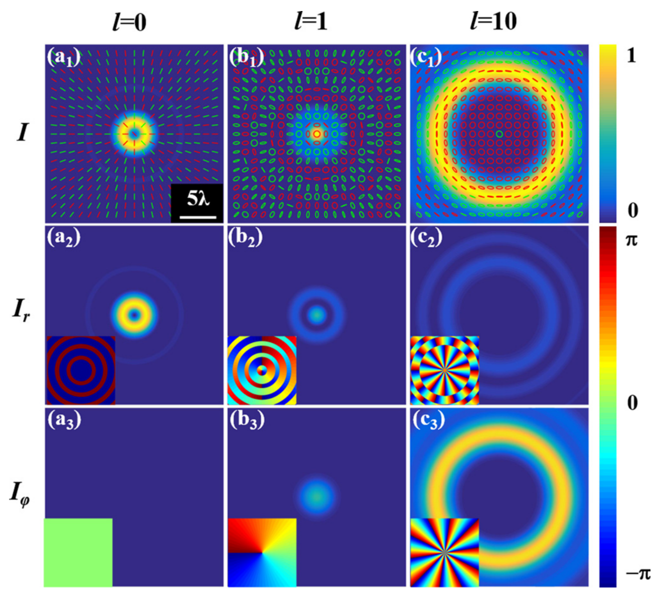

FIG. 3. Calculated intensity, polarization, and phase distributions in the focal plane of radially polarized vortex beams with $l = 0$, 1, and 10, respectively. Top: total transverse components; middle: radial components; and bottom: azimuthal components. The red and green ellipses in top row figures denote the right- and left-hand elliptical polarizations, respectively. The insets in the middle and bottom row display the corresponding phase distributions.

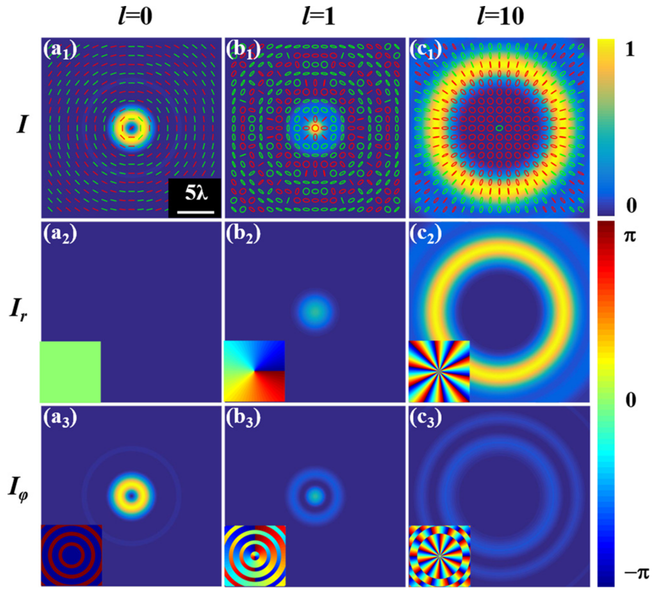

FIG. 4. Calculated intensity, polarization, and phase distributions in focal plane of azimuthally polarized vortex beams with $l = 0$, 1, and 10, respectively. Top: total transverse components; middle: radial components; and bottom: azimuthal components. The red and green ellipses in the top row denote the right- and left-hand elliptical polarizations, respectively. The insets in the middle and bottom rows display the corresponding phase distributions.

has an orientation parallel to the polarization direction of the incident beam.

Figure 4 shows the numerical calculation results of intensity, polarization, and phase distributions in the focal plane of azimuthally polarized vortex beams. The first row shows the total intensity and polarization distributions of focal fields, the middle and bottom rows show the intensity and phase distributions of radial and azimuthal components, respectively. The calculated results demonstrate the polarization conversion from azimuthal polarization to a radial one. That is, as topological charge increases, the intensities of the azimuthally and radially polarized components decrease and increase, respectively, as shown in Figs. 4(a_2)–4(c_2) and 4(a_3)–4(c_3). Similarly, when $l = 1$, the central area where the energy exceeds the ablation threshold is circularly polarized, as shown in Fig. 4(b_1). As a result, the laser-induced surface structure just manifests an ablated hole without ripples, as shown in Fig. 2(b_2). When $l = 10$, the focal field is almost radially polarized as the azimuthal component is almost zero. Therefore, at the focal plane, these two polarization components produce a radial polarization, as shown in Fig. 4(c_1), corresponding to the microstructure in Fig. 2(b_3).

We further explore the influence of topological charges on the morphology. Figure 5 shows the numerically calculated intensity and polarization ellipticity distributions in the focal field of radially and azimuthally polarized vortex beams with $l = 4$ and 8, as well as the SEM images of corresponding microstructures. At the overlapping area of two polarization components, the total fields have linear polarization with orientations perpendicular to the incident conditions. It should be noted that the total focal fields actually have an annular L-line. Especially, for the case of $l = 4$, the polarization state of the annular area with peak energy is elliptically polarized, i.e., the ellipticity is not zero. However, the focal fields can still induce ripples on the silicon surface, whether the incident beam is radial or azimuthal polarized.

In addition, comparing with the polarization states in Figs. 3–5, one can find that the orientation of ripples is always perpendicular to the direction of long axis of the polarization ellipse, evidencing the polarization-locking property. It can also be explained with the interference of the incident beam and SPPs. For elliptically polarized incident beam, the oscillation of excited electrons is not completely definite, but also exhibits a measurement of orientation which is parallel to the long axis of the polarization ellipse. As a result, ripples can also be formed under irradiation of elliptical polarized beam, corresponding to the results in Fig. 5.

Besides the continuous vortex phase, we note that the fan-shaped phase mask and discrete vortex phase have also been introduced to steer the intensity distribution and the conversion of polarization singularities.[29–33] These results support us abundant candidates to further control the morphology. To some extent, in turn, the morphology can delineate the polarization distribution in the context of focal field. Particularly for the measurement of tightly focused fields that are hard to be directly observed, the polarization-locking morphology provides us an indirect scheme.

In summary, we have fabricated surface structures on silicon using focused femtosecond vector vortex beams with different topological charges. The morphology of the surface

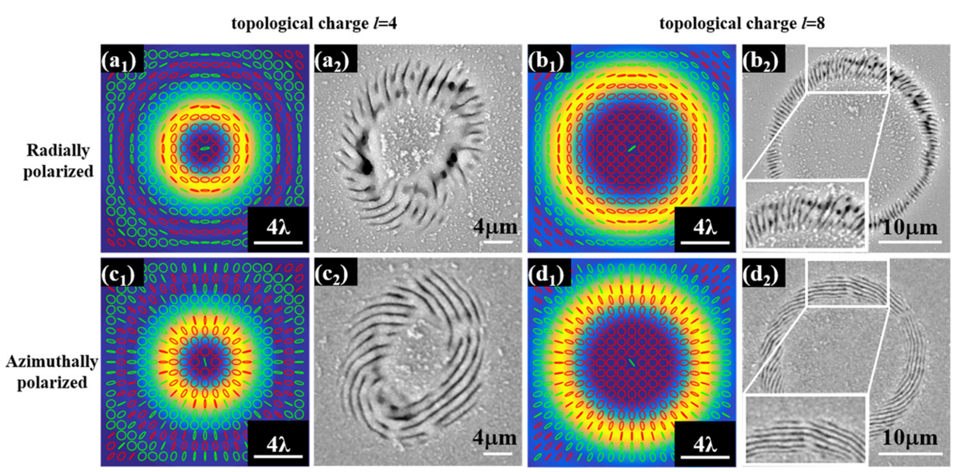

FIG. 5. Calculated intensity and polarization distributions in focal plane and SEM images of the corresponding microstructures. (a), (b) Radially polarized vortex beams with $l = 4$ and 8; (c), (d) azimuthally polarized vortex with $l = 4$ and 8. The red and green ellipses in calculated results denote the right- and left-handed elliptical polarizations, respectively. The long axis of ellipse indicates the azimuthal angle of local polarization.

structures exhibits different shapes and orientations as the topological charges increased, indicating that the vortex-induced morphology conversion of microstructures is achieved. To explain this phenomenon, we calculate the intensity and polarization distributions of corresponding focal fields. It is shown that the focal fields exhibit different polarization directions and ellipticities, compared with the incident fields. As a result, the corresponding microstructures exhibit intriguing morphology different from traditional LIPSS. The focal fields of vector vortex beams demonstrate manageable polarization states and intensity profiles by changing the topological charge, which support a flexible approach in manipulating micro- and nano-scale surface structures.

This work was supported by Joint Fund of the National Natural Science Foundation Committee of China Academy of Engineering Physics (NSAF) (U1630125); the National Key R&D Program of China (2017YFA0303800) and National Natural Science Foundations of China (NSFC) (11634010, 61675168, 11404262, 61377035, and 61575093).

[1]S. Höhm, A. Rosenfeld, J. Krüger, and J. Bonse, J. Appl. Phys. **112**, 014901 (2012).
[2]K. K. Anoop, R. Fittipaldi, A. Rubano, X. Wang, D. Paparo, A. Vecchione, L. Marrucci, R. Bruzzese, and S. Amoruso, J. Appl. Phys. **116**, 113102 (2014).
[3]K. K. Anoop, A. Rubano, R. Fittipaldi, X. Wang, D. Paparo, A. Vecchione, L. Marrucci, R. Bruzzese, and S. Amoruso, Appl. Phys. Lett. **104**, 241604 (2014).
[4]K. Miyazaki and G. Miyaji, J. Appl. Phys. **114**, 153108 (2013).
[5]U. Hermens, S. V. Kirner, C. Emonts, P. Comanns, E. Skoulas, A. Mimidis, H. Mescheder, K. Winands, J. Krüger, E. Stratakis, and J. Bonse, Appl. Surf. Sci. **418**, 499 (2016).
[6]A. Matsugaki, G. Aramoto, T. Ninomiya, H. Sawada, S. Hata, and T. Nakano, Biomaterials **37**, 134–143 (2015).
[7]M. Beresna, M. Gecevičius, P. G. Kazansky, and T. Gertus, Appl. Phys. Lett. **98**, 201101 (2011).
[8]M. Beresna and P. G. Kazansky, Opt. Lett. **35**, 1662 (2010).
[9]W. J. Cai, A. R. Libertun, and R. Piestun, Opt. Express **14**, 3785 (2006).
[10]J. E. Sipe, J. F. Young, J. S. Preston, and H. M. van Driel, Phys. Rev. B **27**, 1141 (1983).
[11]J. Bonse, A. Rosenfeld, and J. Krüger, J. Appl. Phys. **106**, 104910 (2009).
[12]M. Huang, F. Zhao, Y. Cheng, N. Xu, and Z. Xu, ACS Nano **3**, 4062 (2009).
[13]O. Varlamovaa, J. Reifa, S. Varlamovb, and M. Bestehorn, Appl. Surf. Sci. **257**, 5465 (2011).
[14]C. Hnatovsky, V. Shvedov, W. Krolikowski, and A. Rode, Phys. Rev. Lett. **106**, 123901 (2011).
[15]C. Hnatovsky, V. G. Shvedov, and W. Krolikowski, Opt. Express **21**, 12651 (2013).
[16]C. Hnatovsky, V. G. Shvedov, N. Shostka, A. V. Rode, and W. Krolikowski, Opt. Express **37**, 226 (2012).
[17]J. Ouyang, W. Perrie, O. J. Allegre, T. Heil, Y. Jin, E. Fearon, D. Eckford, S. P. Edwardson, and G. Dearden, Opt. Express **23**, 12562 (2015).
[18]K. Lou, S. Qian, X. Wang, Y. Li, B. Gu, C. Tu, and H. Wang, Opt. Express **20**, 120 (2012).
[19]J. J. J. Nivas, S. He, A. Rubano, A. Vecchione, D. Paparo, L. Marrucci, R. Bruzzese, and S. Amoruso, Sci. Rep. **5**, 17929 (2015).
[20]R. Dorn, S. Quabis, and G. Leuchs, Phys. Rev. Lett. **91**, 233901 (2003).
[21]C. Hnatovsky, V. G. Shvedov, W. Krolikowski, and A. V. Rode, Opt. Lett. **35**, 3417 (2010).
[22]K. Toyoda, K. Miyamoto, N. Aoki, R. Morita, and T. Omatsu, Nano Lett. **12**, 3645 (2012).
[23]K. Toyoda, F. Takahashi, S. Takizawa, Y. Tokizane, K. Miyamoto, R. Morita, and T. Omatsu, Phys. Rev. Lett. **110**, 143603 (2013).
[24]D. Barada, G. Juman, I. Yoshida, K. Miyamoto, S. Kawata, S. Ohno, and T. Omatsu, Appl. Phys. Lett. **108**, 051108 (2016).
[25]P. Chen, S. Ge, W. Duan, B. Wei, G. Cui, W. Hu, and Y. Lu, ACS Photonics **4**, 1333 (2017).
[26]P. Chen, W. Ji, B. Wei, W. Hu, V. Chigrinov, and Y. Lu, Appl. Phys. Lett. **107**, 241102 (2015).
[27]W. Ji, C. Lee, P. Chen, W. Hu, Y. Ming, L. Zhang, T. Lin, V. Chigrinov, and Y. Lu, Sci. Rep. **6**, 25528 (2016).
[28]B. Richards and E. Wolf, Proc. R. Soc. London, Ser. A **253**, 358 (1959).
[29]W. Zhang, S. Liu, P. Li, X. Jiao, and J. Zhao, Opt. Express **21**, 974–983 (2013).
[30]X. Jiao, S. Liu, Q. Wang, X. Gan, P. Li, and J. Zhao, Opt. Lett. **37**, 1041 (2012).
[31]P. Li, S. Liu, Y. Zhang, G. Xie, and J. Zhao, J. Opt. Soc. Am. B **32**, 1867 (2015).
[32]P. Li, S. Liu, G. Xie, T. Peng, and J. Zhao, Opt. Express **23**, 7131 (2015).
[33]Y. Zhang, P. Li, S. Liu, L. H. H. Cheng, and J. Zhao, Opt. Express **24**, 28409 (2016).